LANGMUIR

pubs.acs.org/Langmuir Article

X-ray and Neutron Reflectivity Studies of Styrene-Maleic Acid Copolymer Interactions with Galactolipid-Containing Monolayers

Minh D. Phan,*[,⊥] Olena I. Korotych,[⊥] Nathan G. Brady,[⊥] Madeline M. Davis, Sushil K. Satija, John F. Ankner, and Barry D. Bruce*

Cite This: *Langmuir* 2020, 36, 3970−3980 Read Online

ACCESS | Metrics & More | Article Recommendations | Supporting Information

ABSTRACT: Styrene-maleic acid (SMA) copolymers have recently gained attention for their ability to facilitate the detergent-free solubilization of membrane protein complexes and their native boundary lipids into polymer-encapsulated, nanosized lipid particles, referred to as SMALPs. However, the interfacial interactions between SMA and lipids, which dictate the mechanism, efficiency, and selectivity of lipid and membrane protein extraction, are barely understood. Our recent finding has shown that SMA 1440, a chemical derivative of the SMA family with a functionalized butoxyethanol group, was most active in galactolipid-rich membranes, as opposed to phospholipid membranes. In the present work, we have performed X-ray reflectometry (XRR) and neutron reflectometry (NR) on the lipid monolayers at the liquid−air interface followed by the SMA copolymer adsorption. XRR and Langmuir Π−*A* isotherms captured the fluidifying effect of galactolipids, which allowed SMA copolymers to infiltrate easily into the lipid membranes. NR results revealed the detailed structural arrangement of SMA 1440 copolymers within the membranes and highlighted the partition of butoxyethanol group into the lipid tail region. This work allows us to propose a possible mechanism for the membrane solubilization by SMA.

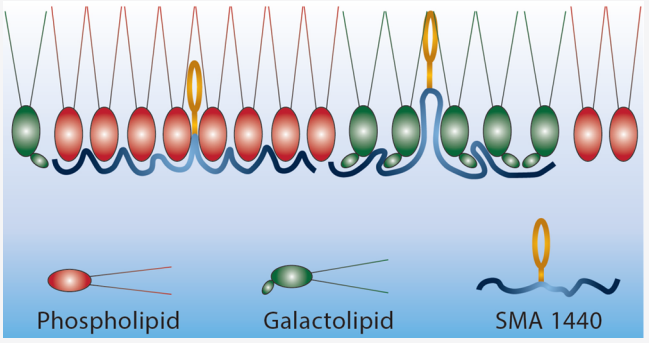

INTRODUCTION

Oxygenic photosynthesis, the process of converting solar energy into biomass and O_2 production, is the main entry of energy into the biosphere and found in all plants, algae, and cyanobacteria. The light reactions of this process take place within galactolipid-rich thylakoid membranes by pigment−protein complexes, termed Photosystems I and II (PSI and PSII). Together the galactolipids (monogalactosyldiacylglycerol, MGDG; digalactosyldiacylglycerol, DGDG; and sulfoquinovosyldiacylglycerol, SQDG) make up between 50 and 70% of the lipids in plants and cyanobacteria.[1] Organization of the thylakoid membranes (TMs) vary from concentric rings paralleling the plasma membrane in cyanobacteria to highly ordered, interspersed disclike stacks called grana in the chloroplasts of higher plants and algae. The distribution of PSII and PSI have been shown to be laterally heterogeneous in both plant chloroplasts[2] and cyanobacteria, forming large arrays of each individual complex with areas where the two occur together to form larger supercomplexes.[3] Thylakoid lipids have been shown to bind in specific pockets at the periphery and interior of photosynthetic protein complexes and be critical for their oligomerization.[3,4] Therefore, these unique lipids have been presumed to be critical to the overall function of these photosynthetic protein complexes *in vitro*.[5]

Styrene-maleic acid (SMA) copolymers with an amphipathic nature are known to extract membrane protein complexes while retaining their surrounding lipids, resulting in more nativelike biophysical characteristics *in vitro*.[6−9] Using SMA provides an opportunity to overcome the disadvantages associated with traditional detergent-based techniques, including possible protein denaturation[7,10,11] and displacement of boundary lipids.[12] The resulting nanosized, protein-containing SMA lipid particles, referred to as SMALPs, can then be used to study membrane proteins in the unamended, proximal environment of the biomembrane.[9,13,14] The consensus thus far in the literature describes membrane solubilization by SMA copolymers as a multistage process. This includes accumulation at the surface up to a critical concentration, followed by insertion and eventual perforation of the biomembrane.[15,16] Interfacial interactions between the lipid membrane and SMA

Received: December 11, 2019
Revised: March 18, 2020
Published: March 24, 2020

https://dx.doi.org/10.1021/acs.langmuir.9b03817
Langmuir 2020, 36, 3970−3980

therefore play a vital role in the mechanism and overall efficiency of the solubilization.

In the present study, we focus on the action of a specific SMA formulation, SMA 1440 (Cray Valley, now part of Polyscope), which has been shown to be effective in extracting pigment protein complexes from galactolipid-rich TM in spinach and cyanobacteria.[17,18] SMA 1440 has a styrene-to-maleic acid ratio (S/MA) of 1.5:1 and is also functionalized with butoxyethanol to increase its hydrophobicity. This butoxyethanol group has also been shown to cause a significant increase in the size of SMA 1440 aggregates, compared to nonfunctionalized polymer by small-angle X-ray scattering. The SMA 1440 self-assembles into prolate ellipsoidal particles approaching 10 nm in diameter, nearly twice the size of more commonly used polymers for the application of membrane solubilization.[19] It is not currently known if this unique topology has a direct effect on the interaction of SMA 1440 with the TMs, but it has been shown that this formulation is most active in galactolipid-rich membranes, as opposed to phospholipid membranes.[18] Not only is the specificity of SMA 1440 for TMs intriguing, but these lipids have been shown to be necessary for the overall function of the photosynthetic reaction center complexes embedded within,[4,20] making the SMALP extraction technique pivotal for studying the primary process of photosynthetic complexes *in vitro*.

X-ray reflectivity (XRR) and neutron reflectivity (NR) are, due to their subnanometer wavelengths and atomic and nuclear sensitivity, ideal to probe interfacial structures and phenomena at the molecular scale.[21,22] In the present work, we have performed XRR and NR for lipid monolayers composed of 1,2-dipalmitoyl-*sn*-glycero-3-phosphocholine (DPPC) and binary mixtures of 80% DPPC with 20% of the following lipids found in TMs: DPPG (dipalmitoyl-*sn*-glycero-3-phospho-(1′-*rac*-glycerol)), MGDG, DGDG, and SQDG. This experimental design allows us to directly interrogate the interaction of SMA copolymer with lipid monolayers at the liquid−air interface before and after the polymer adsorption over top of a well-characterized DPPC background. This approach will allow us to determine the effect of specific lipid classes found in thylakoid membranes, on the mechanism and degree of SMA copolymer association with lipid monolayers. This knowledge may shed light on recent findings, which show the overall efficiency of SMA solubilization is highly dependent on the lipid phase and, particularly, has a strong preference for membranes in a fluid phase.[23]

EXPERIMENTAL SECTION

Materials. Tail-deuterated (d62-) and protiated 1,2-dipalmitoyl-*sn*-glycero-3-phosphocholine (DPPC) and 1,2-dipalmitoyl-*sn*-glycero-3-phospho-(1′-*rac*-glycerol) (DPPG) were purchased from Avanti Polar Lipids (Alabaster, AL, U.S.A.). Digalactosyldiacylglycerol (DGDG) was also purchased from Avanti Polar Lipids. Hydrogenated monogalactosyldiacylglycerol (MGDG) and sulphoquinovosyl diglyceride (SQDG) were purchased from Larodan Research grade Lipids (Monroe, MI, U.S.A.). All lipid structures are depicted in Figure 1. Lipid stock solutions were prepared in chloroform or chloroform/methanol (9:1) (Fisher scientific, Lenexa, KS, U.S.A.) and diluted to 1 mg/mL for experiments. Butoxyethanol ester of styrene-*co*-maleic acid (SMA) copolymer, referred to as SMA 1440 (M_w = 7.0 kDa, M_n = 2.9 kDa) with 1.5:1 S/MA molar ratio (Figure 1), generously gifted by TOTAL Cray Valley (Beaumont, TX, U.S.A.). Hydrochloric acid (Fluka Analytical, St. Louis, MO, U.S.A.), Tris base, and potassium chloride (Sigma-Aldrich, St. Louis, MO, U.S.A.) were used to prepare the subphase buffer. Deionized water from a Barnstead Genpure water purification system (Thermo Scientific, WI, U.S.A.) with a resistivity 18.2 mΩ·m was used to dilute the buffer solution for Langmuir isotherms and X-ray reflectivity experiments, while deuterium oxide (D_2O) (Sigma-Aldrich, St. Louis, MO, U.S.A.) was used to make the buffer for neutron reflectivity experiments. All chemicals and lipids were used without further purification.

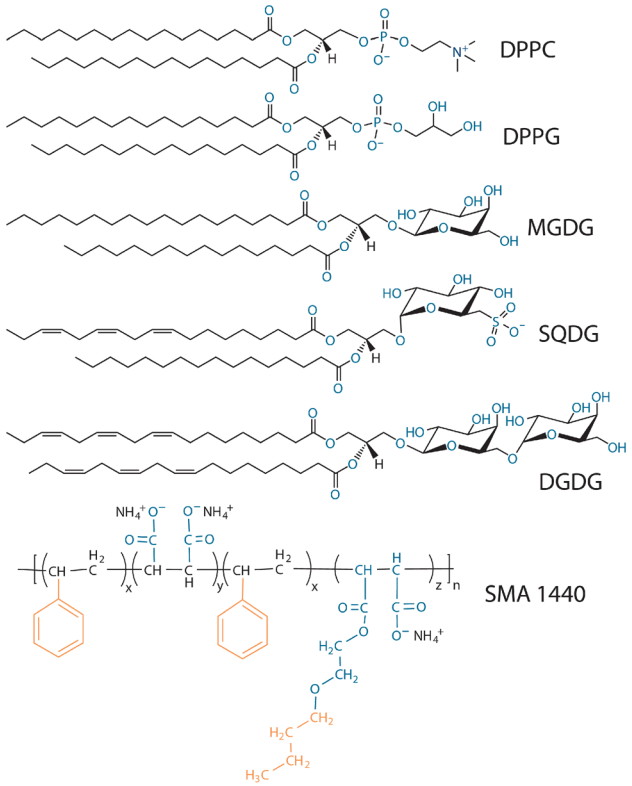

Figure 1. Chemical structures of 1,2-dipalmitoyl-*sn*-glycero-3-phosphocholine (DPPC), 1,2-dipalmitoyl-*sn*-glycero-3-phospho-(1′-*rac*-glycerol) (DPPG), monogalactosyldiacylglycerol (MGDG), sulfoquinovosyldiacylglycerol (SQDG), digalactosyldiacylglycerol (DGDG), and SMA 1440 copolymer. The structures of deuterated DPPC and DPPG are same as the protiated ones but with the fully deuterated tails.

Surface Pressure−Area and Adsorption Isotherms. Surface pressure−area (Π−*A*) isotherms were recorded at a compression rate of 1 mm/min (75 mm^2/min) with two Delrin barriers in symmetric mode by using a Langmuir−Blodgett Deposition trough (KN 2002, KSV NIMA, Helsinki, Finland). The trough was placed in a plexiglass box to prevent air vibration. Before every experiment, the trough and the barriers were cleaned with chloroform and methanol, respectively, using highly adsorbent polyester wipes (AlphaWipe TX1004, Texwipe, Kernersville, NC, U.S.A.), then rinsed thoroughly with deionized water before filling with 1.15 L of filtered SMA buffer (50 mM Tris-Cl and 125 mM KCl) at pH = 9.5 (room temperature) to make a positive meniscus. The subphase was then treated to remove surfactant contaminants until the compression and expansion of the barriers remained at constant pressure (±0.1 mN/m). Lipid samples with a concentration of 1 mg/mL were spread dropwise on the subphase surface with a high-precision Hamilton glass microsyringe (Hamilton, Reno, NV, U.S.A.). After allowing 15 min for the solvent to evaporate and the monolayers to stabilize, compression was initiated. The stability of the entire system was ensured by placing the trough on an active antivibration table (Accurion Halcyonics i4medium, MD, U.S.A.). All isotherms were performed at least twice for each sample to ascertain data reproducibility. The value of surface pressure (Π) was monitored with a filter paper that acts as Wilhelmy plate hanging from a high precision microbalance. Π is

https://dx.doi.org/10.1021/acs.langmuir.9b03817
Langmuir 2020, 36, 3970−3980

Table 1. X-ray Reflectivity Fitting Parameters for the Lipid Membranes before and after the Polymer Adsorption[a]

sample	ρ_p[b]	$\sigma_{p/h}$[c]	t_p[d]	ρ_h	$\sigma_{h/t}$	t_h	ρ_t	$\sigma_{t/a}$	t_t
DPPC				0.43	3.1	7.7	0.34	5.1	17.0
DPPC+SMA				0.42	2.5	9.7	0.34	5.4	17.0
DPPG				0.40	4.1	8.7	0.32	5.3	17.2
DPPG+SMA				0.41	4.1	9.8	0.31	5.2	17.1
MGDG				0.41	3.5	7.3	0.32	4.7	14.1
MGDG+SMA	0.39	2.1	7.6	0.40	3.7	7.2	0.29	4.5	14.8
SQDG				0.42	3.2	6.0	0.33	4.7	14.7
SQDG+SMA	0.37	2.0	11.3	0.39	3.6	5.7	0.31	5.3	14.9
DGDG				0.42	3.5	7.4	0.32	4.7	14.2
DGDG+SMA	0.38	2.0	10.1	0.40	3.3	7.0	0.28	4.0	13.5

[a]The electron density, thickness, and interfacial roughness are denoted by ρ, t, and σ, respectively. The head and tail regions of lipids and polymer are denoted by h, t, and p, respectively. The roughness of the bare buffer−air interface used for all membrane compositions is 3.6 Å, which was obtained by a control measurement for pure buffer before depositing lipid films. [b]The uncertainty of ρ (e^-/Å^3) was <2.5% of the value. [c]The uncertainty of σ (Å) was <±2 Å. [d]The uncertainty of t (Å) was <±0.5 Å.

defined as $\Pi = \gamma_0 - \gamma$, where γ_0 is the surface tension of the bare buffer and γ is the surface tension of the film-covered surface.

Several parameters such as liftoff area (A_L), limiting area (A_∞), and the interfacial elastic modulus of area compressibility (C_s^{-1}) can be extracted directly from the isotherms to discuss the properties of the films. A_L is the mean molecular area at which the isotherms emerge from the baseline, indicating the gas−liquid phase transition. A_∞ is obtained by extrapolating the steepest slope of the isotherm to $\Pi = 0$. Measurement of C_s^{-1} provides insight into the phase transitions and in-plane elastic packing interactions of the monolayers, which are difficult, if not impossible, to obtain by any other techniques. C_s^{-1} is extracted from the isotherm at a given Π by the equation $C_s^{-1} = -A_\Pi(\delta\Pi/\delta A)_T$, where A_Π is the mean molecular area at the corresponding Π. A higher the C_s^{-1} value indicates lower interfacial elasticity.[22,24]

Adsorption isotherms are plotted as the change in Π as a function of time in a fixed-area mode. At the start, lipid monolayers were compressed to $\Pi = 20$ mN/m, at which pressure the films are in a uniformly condensed state. The film was then allowed to relax for 30 min before the barriers were stopped to monitor Π changes following polymer addition. Subsequently, 1 mL of SMA 1440 solution (0.03 wt %) was slowly injected into the subphase underneath the barriers without disturbing the lipid monolayer to a copolymer-to-lipid weight ratio of ∼5 ± 1. Copolymer adsorption reached equilibrium after 3−5 h.

X-ray and Neutron Reflectivity Measurements. XRR measurements were performed at a wavelength of $\lambda = 1.542$ Å from Cu K_α source using D8 Advance reflectometer (Bruker AXS, Karlsruhe, Germany) featuring a vertical goniometer and horizontal sample geometry, allowing the liquid surface to be studied without being disturbed during the measurements. A Langmuir trough (KSV 1000, Helsinki, Finland) with one Teflon barrier for asymmetric film compression was enclosed in a plexiglass box with Kapton windows, through which the X-ray incident and reflected beams pass. The dimensions of the trough were ∼85 × 320 × 4 mm^3 for a total subphase volume of ∼110 mL when filled to a positive meniscus. The entire system was placed on an active antivibration table (Herzan AVI-400, Laguna Hills, CA, U.S.A.). A Cu anode X-ray generator was used to produce Cu K_α radiation, and a parallel incident beam was produced by using a Göbel mirror (GM III). Two slits before the sample defined the size of the incident beam and reduced its vertical divergence. The XRR data were collected in four different constant-q-resolution settings, each of which exceeded what would be needed to resolve the features seen in the data. The reflected intensity was measured as a function of the momentum transfer, $q_z = (4\pi \sin\theta)/\lambda$, where λ and θ are the wavelength and incident angle, respectively. For each sample, we repeatedly varied the incident angle of the beam to measure reflectivity over a range of q_z to monitor thickness and the density changes of copolymer adsorbed at the lipid−liquid interface. Each XRR measurement acquires 3 h including sample alignment and data acquisition. The dispersion, δ, the real part of the X-ray refractive index, is given linearly in terms of the electron density, ρ, by $\delta = (\lambda^2/2\pi)r_e\rho$, where the classical electron radius $r_e = e^2/(4\pi\epsilon_0 mc^2) = 2.814 \times 10^{-5}$ Å. The electron density profiles (ED) shown in this article were calculated from dispersion profiles acquired from fits to X-ray reflectivity data using an exact optical formalism.

NR measurements were performed using the Liquids Reflectometer (LIQREF) at the Spallation Neutron Source (Tennessee, U.S.A.) with a two-dimensional position-sensitive detector. Like XRR, NR measures the neutron reflection as a function of the wavelength (λ) and angle of the beam relative to the sample. Because LIQREF uses a broad neutron spectrum, it can probe a wide q_z range at a single angle of reflection. Therefore, to obtain reflectivity data across a q_z range of 0.008−0.270, only six glancing angles of 0.60°, 0.75°, 1.10°, 1.62°, 2.40°, and 3.20° were used. NR data were collected with a fixed relative resolution, $\delta q/q = 0.05$, better than could be tolerated in the measurements of the thin lipid films. The high q_z regime that had a dominating background was then trimmed off during data reduction. The Langmuir trough was set up similarly to the XRR experiments, except for the following modifications: we used a KSV NIMA trough (KN 1003, Helsinki, Finland) with two Delrin barriers for symmetric compression, which we enclosed in an aluminum box with two quartz windows for the neutron beams to be transmitted in and out. We also supported and stabilized the entire system using a Vario 60 antivibration table (Accurion Halcyonics, MD, U.S.A.). Each NR measurement acquires 1 h including sample alignment and data acquisition.

For both XRR and NR, we used LSFIT,[25] a least-squares fitting routine applying the Levenberg−Marquardt algorithm to fit the data, then confirmed these models with Refl1D.[26,27] In brief, we used the recursive Parratt formalism[28] and the effective-density model[29] to refine a laterally averaged δ for XRR and scattering length density (SLD) for NR profiles perpendicular to the reflecting interface. The effective-density model ensures continuous profiles even if the roughness is not negligible compared to the layer thickness. Sharp interfaces were smeared by a root-mean-square roughness, σ, which was calculated by convoluting a step function with a Gaussian smoothing function. We systematically varied and optimized the fitting parameters (δ or SLD, σ, and thickness t) until the sums of the χ^2-values for all the points on the curve were minimized. We assessed the accuracy of the parameters retrieved from our data refinement by varying the parameters manually and observing the corresponding effect on the calculated reflectivity curve. Since the spatial resolution of XRR benefits from access to a high q-value (0.50 Å^{-1}), the accuracy of the fitting parameters is estimated to be ±2.5% of the value for ρ, less than ±2.0 Å for roughness, and ±0.5 Å for thickness, as depicted in Table 1. On the other hand, NR measurements can only cover up to $q = 0.23$ Å^{-1}, which is insufficient to resolve the full structure of thin lipid films. However, NR is still useful despite the limited q-resolution because of its sensitivity to changes in SLD, which is

https://dx.doi.org/10.1021/acs.langmuir.9b03817
Langmuir 2020, 36, 3970−3980

Table 2. Neutron Reflectivity Fitting Parameters for the Lipid Membranes before and after the Polymer Adsorption[a]

sample	SLD_h	$\sigma_{h/t}$[b]	t_h	SLD_t	$^b\sigma_{t/a}$	t_t
d-DPPC	3.50 ± 0.14	3.2 ± 4.5	7.7 ± 0.7	6.90 ± 0.15	2.8 ± 2.7	16.4 ± 1.3
d-DPPC+SMA	4.20 ± 0.19	3.5 ± 5.7	7.7 ± 1.1	6.40 ± 0.16	3.0 ± 3.8	15.0 ± 2.1
d-DPPG	3.00 ± 0.24	2.4 ± 5.3	6.8 ± 0.8	7.00 ± 0.20	2.3 ± 3.3	17.0 ± 1.8
d-DPPG+SMA	4.20 ± 0.29	3.3 ± 5.6	7.7 ± 0.7	6.40 ± 0.26	4.0 ± 4.3	15.0 ± 1.8
MGDG	3.14 ± 0.24	2.6 ± 4.4	6.9 ± 0.7	6.10 ± 0.29	2.3 ± 3.8	15.2 ± 1.7
MGDG+SMA	3.87 ± 0.25	2.9 ± 4.3	6.9 ± 0.9	6.13 ± 0.27	2.6 ± 3.9	15.2 ± 2.3
SQDG	2.71 ± 0.18	3.1 ± 4.4	6.5 ± 0.8	5.26 ± 0.24	2.6 ± 5.9	15.5 ± 1.4
SQDG+SMA	3.29 ± 0.21	2.5 ± 6.0	4.4 ± 1.1	5.60 ± 0.22	2.5 ± 4.8	15.5 ± 2.1
DGDG	2.99 ± 0.12	2.6 ± 6.2	6.5 ± 1.0	5.58 ± 0.23	2.2 ± 4.8	15.5 ± 1.5
DGDG+SMA	3.20 ± 0.12	3.4 ± 5.8	6.5 ± 0.9	5.90 ± 0.26	2.6 ± 4.5	15.5 ± 1.6

[a]The scattering length density, thickness, and interfacial roughness are denoted by SLD, t, σ, respectively. The head and tail regions of lipids are denoted by h and t, respectively. The roughness of the bare buffer−air interface used for all membrane compositions is 2.0 Å, which was obtained by a control measurement for pure D_2O-based buffer before depositing lipid films. [b]The relatively large uncertainty of σ (Å) was the result of the statistical uncertainty of the data at $q > 0.15$ Å^{-1} and the limited q range of NR measurements to read the full thin film thickness.

proportional to the reflected intensity at the low-statistical-uncertainty q-region (0.10−0.15 Å^{-1}). Therefore, the structural parameters (thickness and roughness) obtained from NR are not well-defined as the SLD, which is presented by the uncertainty levels shown in Table 2.

RESULTS AND DISCUSSION

Effect of Different Lipid Classes on the Physical Properties of Monolayers. The scope of our work is to understand the fundamental effects of each lipid class present in TMs, including galactolipids (MGDG, DGDG, and SQDG) and phospholipids (PC and PG).[1] Specifically, we focus on membrane structural and physical properties, as well as on the interaction with SMA copolymers to account for the SMA extraction function. Therefore, it is not necessary to choose a realistic compositions mimicking TMs.

DPPC was chosen to represent the PC lipid class in TMs because it is one of the most well-characterized phospholipids,[21,22,30] whose headgroup carries no net charge, and whose acyl chains are fully saturated. At 80 mol %, DPPC is expected to dominate the structural properties of the membrane and form a well-packed membrane structure, which provides a baseline for comparing the membrane structural effects of the 20 mol % secondary components in the binary mixtures, including the charged headgroups of DPPG and SQDG, as well as the galactosyl rings in the MGDG, SQDG, and DGDG headgroups. We also chose hydrated MGDG, a galactolipid with fully saturated acyl chains, as an intermediate between the fully saturated phospholipids and the unsaturated galactolipids (Figure 1). (Hereafter, DPPC 100 mol % will be termed DPPC, and binary mixtures will be referenced by the second component: DPPG, MGDG, SQDG, and DGDG).

The Langmuir isotherm is routinely used to determine molecular interactions occurring in monolayers at the liquid−air interface. As shown in Figure 2A, the observed liftoff area A_L, the packing density at which molecules begin interacting with each other, for individual mixtures increased in the following order: MGDG ≪ DPPC = DGDG < SQDG < DPPG. Since DPPC and DPPG have identical acyl chains, it is not surprising that DPPG, bearing a negatively charged headgroup, has a larger A_L value than the zwitterionic DPPC due to mutual repulsion of those headgroups. However, it is interesting that bulky galactosyl rings on the headgroup of the galactolipid did not increase A_L values in comparison to the phospholipids. Also, the A_L value for MGDG with fully saturated acyl chains ≪ DPPC < MGDG with highly unsaturated acyl chains (Figure S1), indicating that the acyl chains contribute to the value of A_L and that a free, saturated MGDG molecule is more compact than DPPC. Note that the gas state features the most intrinsically stable structure of a molecule due to the lack of intermolecular interactions.

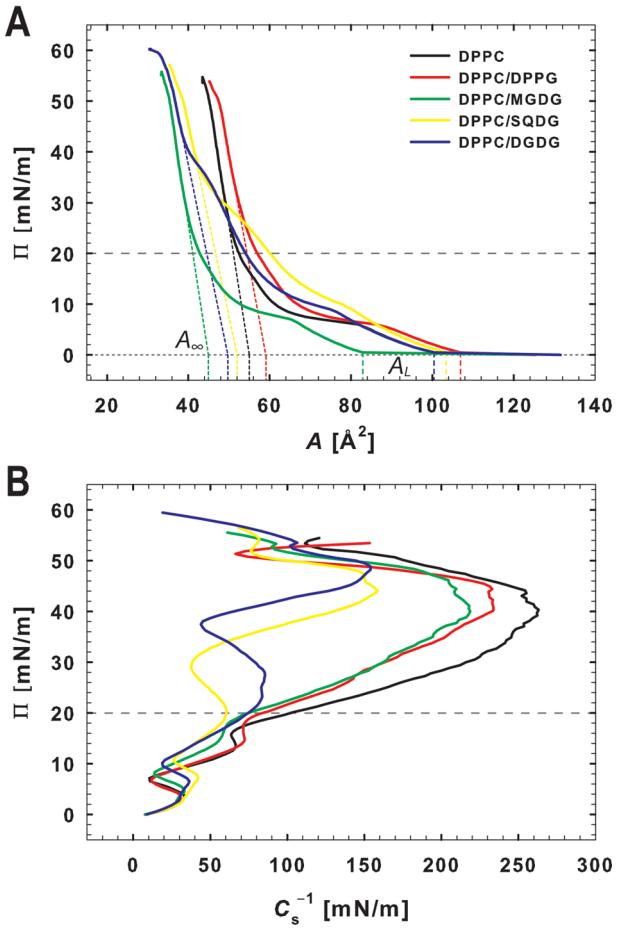

Figure 2. (A) Surface pressure−area (Π−A) isotherms and (B) surface pressure−elastic modulus of area compressibility (Π−C_s^{-1}) plots of DPPC and binary mixtures composed of 80 mol % DPPC and 20 mol % other lipid component, either phospholipid or galactolipids, performed on the H_2O-based buffer. The dashed lines extrapolate the isotherms at the steepest slope to determine the limiting area A_∞. The horizontal dashed lines in both panels represent Π = 20 mN/m to provide a visual guide.

https://dx.doi.org/10.1021/acs.langmuir.9b03817
Langmuir 2020, 36, 3970−3980

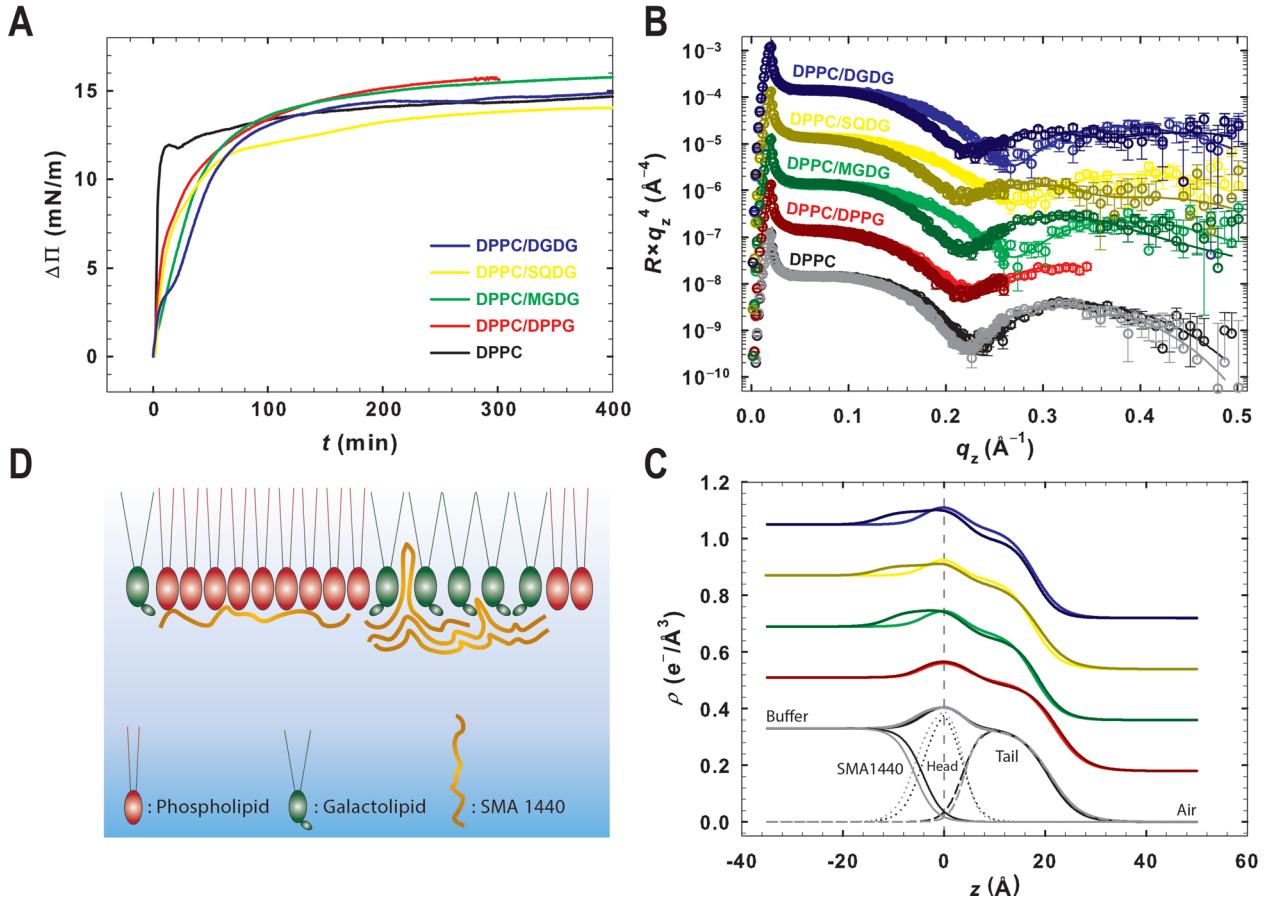

Figure 3. (A) Adsorption isotherms of SMA 1440 on DPPC and the binary mixtures composed of 80 mol % DPPC and 20 mol % another lipid component, either phospholipid or galactolipids, in the H_2O-based buffer. The isotherms are plotted by $\Delta\Pi = \Pi_t - \Pi_0$ in which $\Pi_0 = 20$ mN/m, as a function of time. (B) X-ray reflectivity data for the lipid membranes before (vivid colors) and after (grayed colors) the introduction of copolymer at the equilibrium state. The lines through data were obtained by using an iterative procedure and are best fits resulting in (C) the corresponding model electron density (ED) profiles. The reflectivity signal from the interfaces, R, is plotted on a semilog scale as $R \times q_z^4$ to amplify the modulations for more accurate comparison. (C) ED profiles along the surface depth, where zero position is assigned to the location of the lipid headgroup before the introduction of the copolymer. The lightweight solid, dotted, and dashed lines at DPPC SLD profiles are the deconvoluted profiles for the subphase, lipid headgroup, and tail regions, respectively. (D) Schematic presentation of SMA binding differently to phospholipid- and galactolipid-rich domains.

Therefore, it is possible that galactolipids in the gas phase (without intermolecular interaction) align their bulky galactosyl rings vertically with the acyl chains and minimize their lateral occupation at the liquid−air interface. In contrast to A_L, A_∞ features packing structures regulated by intermolecular interactions. The observed A_∞ for individual mixtures increased in the following order: MGDG < DGDG < SQDG < DPPC < DPPG, suggesting that it is harder to compress the galactolipid-containing monolayers to the closely packed state in comparison to the phospholipid monolayers. These data also suggest that the negatively charged sulfonate on SQDG is "bulkier" than the second galactosyl group of DGDG.

At ∼6 mN/m, Π−A behavior of DPPC shows a sharp inflection, indicative of the onset of a two-dimensional phase transition into a more chain-ordered, condensed state (Figure 2A). Not surprisingly, a sharp drop in C_s^{-1} values occurred at Π between 4 and 7 mN/m before reversing sign and increasing to values more characteristic of a condensed phase at higher Π (Figure 2B). The dramatic drop in C_s^{-1} values reflects discontinuities in lateral packing at phase boundaries and accompanying lateral density fluctuations that are known to occur when liquid-expanded (LE) and liquid-condensed (LC) phases coexist. For this reason, the plot of Π−C_s^{-1} proved to be an informative way to recognize the Π range over which fluid and condensed phases coexist. These observations are in general agreement with previous reports,[22] allowing for small variations resulting from differing buffer conditions. An unusual second kink in DPPC's Π−A at ∼16 mN/m shown in Figure 2A corresponds with a sharp drop in C_s^{-1} at Π between 13 and 15 mN/m and indicates a transition from LC to a solid phases, possibly resulting from the basic buffer condition (pH 9.5).

As shown in Figure 2B, the Πs at which the LE−LC phase transition appears is in the following order: DPPC = DPPG < MGDG < DGDG < SQDG, suggesting that the galactosyl rings increase the overall fluidity of the films at the LE-LC transition. The Π sequence for the LC-S transition is in the following order: DPPC < DPPG ∼ MGDG ≪ SQDG ≪ DGDG, suggesting that both acyl chains and headgroups contribute to the overall phase behavior. This also suggests that the fluidifying effect of galactosyl becomes more pronounced, making DGDG and SQDG remarkably harder to condense into the solid-state. At Π = 20 mN/m, SQDG and

https://dx.doi.org/10.1021/acs.langmuir.9b03817
Langmuir 2020, 36, 3970−3980

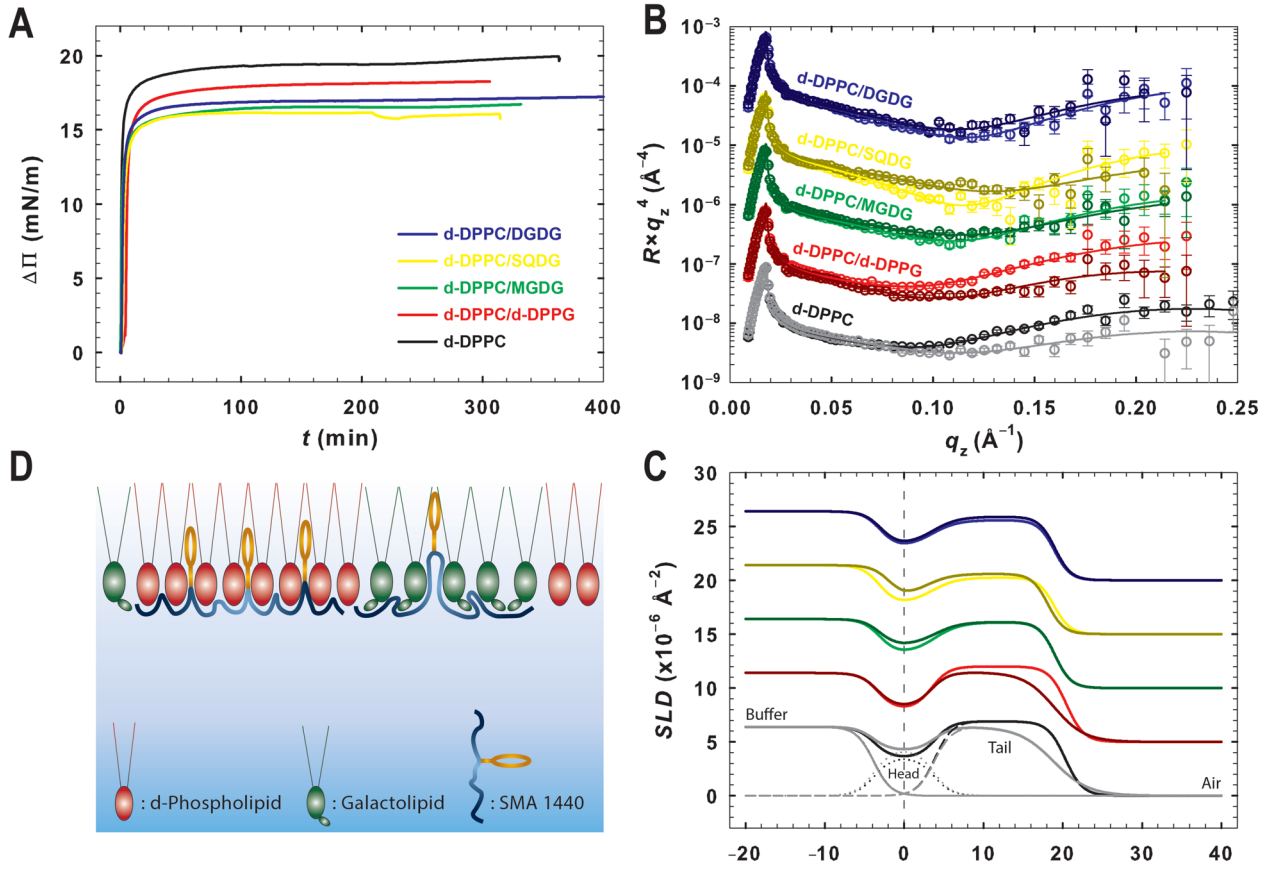

Figure 4. (A) Adsorption isotherms of SMA 1440 on d-DPPC and the binary mixtures composed of 80 mol % d-DPPC and 20 mol % another lipid component, either d-DPPG or galactolipids in the D_2O-based buffer. (B) Neutron reflectivity data for the lipid membranes before (vivid colors) and after (grayed colors) the introduction of copolymer solution at the equilibrium state. The lines through data were obtained by using an iterative procedure and are best fits resulting in (C) the corresponding model scattering length density (SLD) profiles. The reflectivity signal from the interfaces, R, is plotted on a semilog scale as $R \times q_z^4$ to amplify the modulations for more accurate comparison. (C) SLD profiles along the surface depth, where the zero position is assigned to the location of the lipid headgroup before the introduction of copolymer. The lightweight solid, dotted, and dashed lines at DPPC SLD profiles are the deconvoluted profiles for the subphase, lipid headgroup, and tail regions, respectively. (D) Schematic presentation of SMA insertion into the deuterated phospholipid- and galactolipid-rich domains.

DGDG had not reached the second phase transition, while DPPC, DPPG, and MGDG were increasing in C_s^{-1} to values more characteristic of a condensed state, and the observed C_s^{-1} sequence was SQDG < DGDG ~ MGDG < DPPG < DPPC.

The excess Gibbs free energy of mixing, G_E, is used to estimate the thermodynamic miscibility of the two-component mixtures.[22] As shown in Figure S2, a DPPC/DPPG mixture at 80/20 molar ratio possesses slightly positive G_E values, 0 kJ/mol < G_E < 0.12 kJ/mol, over the entire Π range, suggesting mixing is not thermodynamically favored. This result is not consistent with previous reports,[31,32] which showed a nearly ideal mixed system. This discrepancy may be attributed to the high pH subphase (pH 9.5, 50 mM Tris-Cl, and 125 mM KCl), which was chosen based on the working extraction condition of SMA 1440 copolymers in photosystems.[17,18]

For the galactolipids, although several works earlier reported Π–*A* isotherms of the pure MGDG and DGDG,[33−35] we could not fabricate stable monolayers of any galactolipids with reproducible Π–*A* isotherms under high pH subphase conditions. The instability of pure galactolipid monolayers may be attributed to a predominantly nonlamellar phase as already observed for saturated MGDG.[33,34] Without the isotherms of the pure galactolipids, we, therefore, could not estimate thermodynamic miscibility for galactolipid-containing films. However, in those reports that successfully fabricated stable pure galactolipid monolayers, the Π–*A* isotherms showed no phase transition and remained in a disordered phase over the entire compression range, which was consistent with our unreproducible isotherms. As shown in Figure 2, the two phase-transitions of pure DPPC are present in all of the Π–*A* isotherms of the galactolipid-containing membranes, suggesting a presence of segregated DPPC-rich domains. These transitions, however, emerge at higher Π, indicating that some galactolipids may have been recruited into the DPPC-rich domains and partially fluidified the ordered phase.

Adsorption Behavior and Changes in Interfacial Structure. To estimate the degree and kinetics of SMA copolymer adsorption to the membrane, we recorded Langmuir adsorption profiles. After the membrane monolayer had been compressed and stabilized at Π = 20 mN/m, the copolymer solution was introduced into the H_2O-based buffer subphase via injection under the trough barriers to avoid disturbing the membrane. Since this study aims to elucidate the binding behavior of SMA to the lipid interface as part of its solubilizing mechanism, the adsorption isotherms were measured in a fixed area mode to prevent membrane expansion and contraction and to monitor the change in Π as a function of time.

https://dx.doi.org/10.1021/acs.langmuir.9b03817
Langmuir 2020, 36, 3970−3980

As shown in Figure 3A, all adsorption profiles generally begin with a steep increase in Π until reaching a saturated equilibrium. This behavior is consistent with the adsorption of SMA 1440 copolymers to the bare buffer−air interface (without lipids) shown in Figure 5 below. If that interface is fully covered by well-packed lipid monolayers, suppressing the migration of SMA 1440 copolymers all the way to the surface, then a lower maximum Π is seen in adsorption assays compared to that measured for the bare surface. Logically, the copolymers first interact with lipid headgroups and then insert the hydrophobic moieties into the tail regions. The interaction with the lipid headgroups may be either via electrostatic attraction with PC, which is accounted for 80% of the total lipids, or via a simple hydrophilic interaction with all the lipid headgroups. The former argument is better supported by the adsorption assays in Figure 3A (and Figure 4A below), where both kinetics and the maximum Π value for pure DPPC is highest among all the membrane compositions although at 20 mN/m DPPC is in its most condensed state compared to the binary mixtures (Figure 2B).

XRR at the liquid−air interface was performed to probe the structural changes of the lipid membranes and adsorbed copolymer during the adsorption assay recorded in Figure 3A. XRR measures the intensity of X-rays reflected from an interfacial surface as a function of the momentum transfer vector $q_z = (4\pi \sin \theta)/\lambda$, where λ is the X-ray wavelength. This intensity versus incident angle relationship is essentially an interference pattern produced by variations in the one-dimensional ED profile along with the dimension perpendicular to the reflecting interface averaged over the in-plane dimension parallel to the reflecting interface. The q_z value of the minimum reflectivity in these profiles is proportional to the inverse of the total layer thickness so the magnitude of the change in q_z can be used to track changes in layer thickness.

Figure 3B presents the XRR profiles taken at the equilibrium states of each lipid composition before and after the introduction of the copolymer solution. Compared to DPPC, the oscillation of DPPG's profile shifts slightly to a lower q_z, whereas those of the galactolipids' profiles shift significantly to higher q_z values, indicating that the galactolipids fluidified the ordering and caused the membrane thinner. These results are opposite from the earlier report by Watkin et al. where the glycolipids with the bulky carbohydrate structure in the headgroup enhanced the ordering of surrounding DPPC in monolayers,[36] given that the carbohydrate and galactosyl in galactolipids are structurally similar. The overall thickness order of the bare membrane (preinjection) was DPPG > DPPC > MGDG ∼ SQDG ∼ DGDG.

In contrast to the adsorption profiles (Figure 3A), the amount of adsorbed copolymer does not cause much change in the membrane structures composed of only phospholipids, evidenced by a slight shift of the oscillation at q_z∼ 0.22−0.24 to a lower value. For the galactolipid-containing membranes, the oscillations shift more significantly to lower q_z values, indicative of preferential copolymer association with galactolipids over phospholipids. There are no additional oscillations in any XRR data emerging at a low q_z regime, suggesting that the copolymer association in all membrane compositions is rather local and insufficient to form a uniform layer beneath the membranes.

On the basis of the observations above, a three-layer model, including two layers accounting for the lipid membrane (head and tail regions) and one layer accounting for the associated copolymer, was applied to fit the galactolipid-containing profiles. In contrast, a two-layer model, including head and tail regions, was used for the phospholipid profiles. The ED profiles are shown in Figure 3C, and a full table of fitting parameters is presented in Table 1. The pure DPPC membrane yields mean values of 7.7 and 17.0 Å for the thickness and 0.43 and 0.34 $e^-/Å^3$ for the ED of the lipid headgroup and tail regions, respectively. These values are in general agreement with previously measured values for DPPC monolayers, allowing for small variations resulting from experimental conditions.[21,22] After the introduction of the copolymer, the entire membrane structure remains the same, except for an increased thickness of the headgroup region by 2.0 Å and the ED value decreasing by 0.01 $e^-/Å^3$ (2.3%). These structural changes are attributed to copolymer molecules locally adsorbing to the membrane surface. Likewise, the adsorbed copolymer slightly increases the ED by 2.5% and thickness of DPPG's headgroup region by ∼1 Å, while decreasing the ED value of the tail regions by 3.1%.

Bare MGDG yields thickness values of 7.3 and 14.1 Å and 0.41 and 0.32 $e^-/Å^3$ for the ED of the headgroup and tail regions, respectively, which are smaller than those of pure DPPC, despite having similar, fully saturated acyl chains. The overall thickness of all galactolipid-containing membranes is about the same. These results confirm that the flexible nature of the galactosyl ring discussed in Figure 2B dictates the packing capacity of MGDG, SQDG, and DGDG.

Binary mixtures with galactolipids exhibit more drastic structural changes upon copolymer association than those composed solely of phospholipids. For MGDG, the adsorbed copolymer molecules decrease the thickness of the headgroup and ED of both headgroup and tail regions, together with a formation of 7.6 Å and 0.39 $e^-/Å^3$ copolymer layer. The decrease in ED of the lipid's headgroup and tail regions occurs for all galactolipid-containing membranes upon copolymer adsorption, revealing an interruption of membrane packing density caused by copolymer insertion. Note that the decreased ED of the tail region obtained from the XRR fit can only be attributed to a decrease in packing density of the tails because the insertion of both hydrophobic and/or hydrophilic moieties without disrupting the packing would lead to an increased ED value. Also, copolymer molecules accumulate more on SQDG and DGDG monolayers, 11.3 and 10.1 Å, respectively, compared to MGDG, which correlates with the degree of fluidity discussed in Figure 2B.

The schematic depicted in Figure 3D summarizes the differences in SMA copolymer interactions with phospholipid and galactolipid-containing membranes. The inserting configuration of copolymer into the galactolipids, resulting from the flexible character of galactosyl rings, seems to be a pivotal factor in facilitating the accumulation of copolymer molecules on the membrane surface.

Adsorption Behavior in D_2O-based Buffer and the Detailed Distribution of Copolymers within Membranes. Figure 4A shows the adsorption profiles of pure deuterated DPPC (d-DPPC) and binary mixtures containing 80 mol % d-DPPC and 20 mol % of other components, for example, deuterated DPPG (d-DPPG) and protiated MGDG, SQDG, and DGDG. The general trend observed in H_2O buffers is well preserved for all of the adsorption profiles in D_2O, except that the initial increments of Π are much steeper (nearly vertical for all membrane compositions) and end at a higher value, which is consistent with the adsorption behavior

https://dx.doi.org/10.1021/acs.langmuir.9b03817
Langmuir 2020, 36, 3970−3980

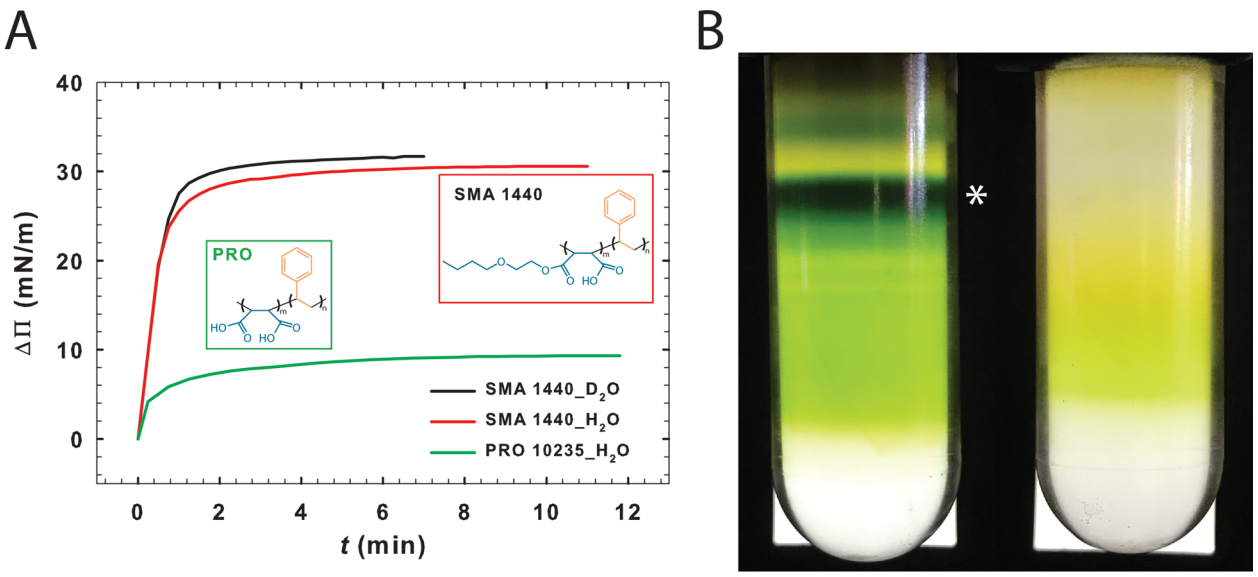

Figure 5. (A) Surface-active properties of SMA 1440 in both H_2O- and D_2O-based buffers in comparison with PRO 10235 in the H_2O-based buffer. (B) Solubilization performance of SMA 1440 versus PRO 10235 in the thermophilic cyanobacterium *Thermosynechococcus elongatus*. Both copolymers have the same styrene-to-maleic acid ratio of 1.5:1 but SMA 1440 has the functionalized butoxyethanol group, while PRO 10235 does not. The asterisk marks photosystem I trimers.

of SMA 1440 copolymers in the D_2O- versus H_2O-based buffer to the bare interface (Figure 5 below). These isotopic discrepancies are due to the nature of the O—D bond being less polar than O—H decreases the hydration effect of D_2O from that of H_2O and thereby increases the activity of the negative charge on the maleic group of the copolymer in D_2O-based buffer. Also, it was reported earlier that the LE−LC phase transition of d-DPPC occurs at a higher Π than that of protiated DPPC, indicating d-DPPC lipids pack less effectively than protiated DPPC.[30]

As with XRR, NR also measures the SLD profile along the dimension normal to the reflecting interface averaged over the in-plane dimension. Unlike XRR, NR cannot reach sufficient q to resolve the added thickness of adsorbed copolymers to the thin lipid monolayers. However, NR is superior for obtaining the detailed copolymer distribution within the membrane owing to the large SLD contrast between the individual moieties of SMA copolymer, lipid headgroup, and hydrocarbon tail regions. NR measurements were performed in a D_2O-based buffer using d-DPPC as a backbone for all the binary mixtures to enhance the SLD contrast between the membrane monolayer and the neutron transmitting medium, which is air.

In Figure 4B, the NR profiles taken at the equilibrium states show sufficiently clear changes in the reflected intensity upon copolymer adsorption to enable us to infer changes in the SLD profiles. Note that the calculated NR curves for the 25 Å thick bare lipids and additional 10 Å thick adsorbed copolymers show oscillations at q of 0.37 and 0.30 $Å^{-1}$, respectively, which is a practical challenge to reach due to the incoherent background by protons and deuterons. Therefore, relying primarily on the reflected intensity to infer changes in SLD profiles was the most reliable approach to analyze the NR data. The changes in reflected intensity were adequate for DPPC, DPPG, and SQDG, and less so for MGDG and DGDG. However, with the supporting pieces of evidence from XRR and the adsorption assay, we could safely presume that there were copolymers associated with MGDG- and DGDG-containing membranes despite the small changes observed in NR profiles.

The adsorbed copolymer decreased the reflected intensity of the NR profiles for phospholipids, yet increased intensity for galactolipids when compared to the corresponding bare membranes. Note that SMA 1440 monomer consists of three structural units, including styrene, negatively charged maleic acid, and butoxyethanol with calculated SLD values of 1.22, 2.88, and $-0.04 \times 10^{-6}/Å^2$, respectively. Hydration effects could lead to underestimation of the SLD of the maleic acid and butoxyethanol units of SMA 1440. The butoxyethanol functionality also has a terminal hydrophobic butane group that could readily intercalate into the acyl tail region of the monolayers.

Accordingly, the SLD profiles shown in Figure 4C were obtained by fitting the NR profiles with a two-layer model for all membrane compositions. SMA association accounts for the changes in SLD of the headgroup and tail regions. Because of the limited q-range and low binding densities of SMA to the lipid membranes, NR measurements are not sensitive to the structure of the adsorbed copolymer. Therefore, the two-layer and three-layer fitting models do not make significant difference (Appendix and Figure S3 in SI). The fitting parameters are outlined in Table 2. In all cases, the adsorbed copolymers enhance the SLD of the headgroup, suggesting maleic acid, the high SLD and hydrophilic component of SMA, resides in this region. Also, maleic acid unit ($C_4H_2O_4$), being relatively H-poor, has a higher neutron scattering length than the other lipid headgroups (DPPC−$C_{10}H_{18}NO_8P$; DPPG−$C_8H_{12}O_{10}P$; MGDG−$C_{11}H_{16}O_{10}$; SQDG−$C_{11}H_{32}NO_{12}S$; and DGDG−$C_{17}H_{27}O_{15}$). Having maleic moieties reside at the lipid headgroups, therefore, increases the SLD of the headgroup layer. For the phospholipid membranes, the SLD of the tail regions decreases, together with the increase in the roughness values of headgroup−tail and tail−air interfaces upon the SMA copolymer adsorption. These results suggest that the insertion of styrene, a nonhydrated, low-SLD, and

https://dx.doi.org/10.1021/acs.langmuir.9b03817
Langmuir 2020, 36, 3970−3980

hydrophobic component of SMA, into the tail region disrupts the packing density of the membranes.

While MGDG exhibits no significant change, the SLD of other galactolipid membranes' tails increases, indicating penetration of hydrated butoxyethanol due to its hydrophobic character into the galactolipid's tail region. Since styrene is a hydrophobic-driven unit and has been shown to insert into more compact phospholipids, tails, we cannot preclude the possibility of styrene also inserting into the galactolipid's tail region.

For the MGDG-containing membrane, 80 mol % of DPPC should have shown a decrease in SLD of the tail layer as observed in the pure d-DPPC, if there was no D_2O in the form of hydration shell present in the MGDG's tail. It is therefore possible that the hydrated butoxyethanol had been inserted into the MGDG tail layer but to a lesser degree in SQDG and DGDG tail layers. The schematic in Figure 4D depicts different inserting configurations of SMA copolymer within the phospholipid- and galactolipid-containing domains. The golden ring denotes the styrene, while the blue gradient section denotes the hydrated moieties including maleic acid and butoxyethanol groups.

We have characterized the effects of phospholipid and galactolipid classes on the structural and physical properties of the membranes as well as on SMA copolymer adsorption. Although the uses of deuterated lipids and D_2O in the NR experiments slightly altered the packing density of the lipid membranes and the interaction between the membranes and SMA 1440 copolymers, making XRR and NR results inconsistent, the two techniques are nonetheless still complementary to provide a complete picture of SMA 1440 action. Particularly, XRR, while insensitive to subtle compositional details within the film, with access to high q-value can determine SMA adsorption in terms of total film thickness. NR, although it cannot capture a full film thickness fringe due to its limited q-range, is sensitive to small changes in SLD that allow us to infer the structural distribution of SMA 1440 copolymer within the membrane monolayers. As shown in the NR data, these structural distributions are lipid class (phospholipid versus galactolipid) dependent and are not affected by deuteration.

As a result, DPPC-enriched domains possess a well-packed membrane structure, while negatively charged DPPG and SQDG, as well as the bulky galactosyl groups on galactolipids, disrupt the packing of the headgroup (Figure 2B). The galactosyl groups disrupt the headgroup packing drastically, enough to promote the association of both phenyl groups and hydrated butoxyethanol into the membrane hydrophobic tails (Figure 4C). The insertion of hydrated butoxyethanol could be critical as it has been recently reported that SMA 1440 functionalized with butoxyethanol showed higher activity with TM and increased the size of extracted SMA lipid particles, compared to nonfunctionalized polymer.[19,37] In all membrane compositions, the carboxyl groups of maleic acid reside in the headgroup region, in agreement with previous reports.[16,38]

To highlight the amphiphilicity enhanced by the butoxyethanol group, we have performed the adsorption assay comparison between SMA 1440 and PRO 10235, which is structurally similar to SMA 1440 but has no functionalized butoxyethanol group, to the bare liquid−air interface (without the lipids). As shown in Figure 5A, the number of copolymers arriving at the interface defined by the maximum Π for SMA 1440 is three-times higher than that for PRO 10235. The insertion of butoxyethanol concluded by NR data sheds light on the solubilization performance of SMA 1440 and PRO 10235, where the two copolymers are used to solubilize the photosystem I (PSI) trimers from thylakoid membranes of the thermophilic cyanobacterium *Thermosynechococcus elongatus*. As depicted in Figure 5B, PRO 10235 did not solubilize the PSI trimers embedded in galactolipid-rich membranes, while SMA 1440 showed excellent efficiency in extracting PSI trimers with surrounding native thylakoid membranes.

The specific action of SMA copolymers on binary mixed membranes could be postulated as follows: The amphiphilic nature of SMA copolymers is a main driving force that enables the copolymers to the lipid membranes spontaneously. At the lipid−air interface, the electrostatic interaction with DPPC-enriched region could be crucial for the copolymer initial accumulation. The binding copolymers then laterally move while trying to insert at least the styrene moiety into the membrane. The flexible galactosyl groups cause disordering to the galactolipid-enriched domains that facilitates the deeper insertion of phenyl and hydrated butoxyethanol into the galactolipid tails. Despite the fast kinetics of SMA 1440 arriving at the bare liquid−air interface, in minute-time scale (Figure 5A) SMA association into the lipid membranes could take hours. For instance, the SMA 1440 association into the SQDG-containing membrane reaches an equilibrium after 4 h, as shown in Figure S4.

CONCLUSIONS

SMA 1440 copolymers spontaneously arrive at the lipid membrane surface due to the strong surface-active property. At the interface, the electrostatic interaction with PC headgroups hold the copolymers at the lipid membrane. SMA copolymers then insert at least the styrene moiety into the acyl chain region of the lipids to maximize the hydrophobic interaction. The degree of styrene insertion into the phospholipid tail region is dependent on the packing density of the membrane. In galactolipid-enriched domains, flexible galactosyl rings impart fluidity to the structural and physical behaviors of the membrane, promoting the deep insertion of phenyl and hydrated butaxyethanol into the hydrophobic tail region. These results provide a fundamental understanding of recent work, which shows SMA 1440 is most active in galactolipid-rich membranes, as opposed to phospholipid membranes.[18] Also, these experimental findings are well aligned with previous theoretical reports and therefore establish the initial steps of the membrane solubilization mechanism of SMA copolymers.

ASSOCIATED CONTENT

Supporting Information

The Supporting Information is available free of charge at https://pubs.acs.org/doi/10.1021/acs.langmuir.9b03817.

> Langmuir Π−*A* isotherms of unsaturated MGDG and DPPG, the calculated excess Gibbs free energy of mixing and excess area for DPPC/DPPG mixture, and the adsorption assay of SMA 1440 in both H_2O- and D_2O-based buffer, versus PRO without functionalized butoxyethanol group to compare the surface action with SMA 1440, to the bare interface without lipid films (PDF)

https://dx.doi.org/10.1021/acs.langmuir.9b03817
Langmuir 2020, 36, 3970−3980

AUTHOR INFORMATION

Corresponding Authors

Minh D. Phan − *Large-Scale Structures Group, Neutron Scattering Division, Oak Ridge National Laboratory, Oak Ridge, Tennessee 37830, United States;* orcid.org/0000-0002-6132-5277; Email: phanmd@ornl.gov

Barry D. Bruce − *Department of Biochemistry, and Cellular, and Molecular Biology and Department of Microbiology, University of Tennessee at Knoxville, Knoxville, Tennessee 37966, United States;* orcid.org/0000-0002-4045-9815; Email: bbruce@utk.edu

Authors

Olena I. Korotych − *Department of Biochemistry, and Cellular, and Molecular Biology, University of Tennessee at Knoxville, Knoxville, Tennessee 37966, United States;* orcid.org/0000-0002-0835-2305

Nathan G. Brady − *Department of Biochemistry, and Cellular, and Molecular Biology, University of Tennessee at Knoxville, Knoxville, Tennessee 37966, United States;* orcid.org/0000-0002-3443-8006

Madeline M. Davis − *Department of Biochemistry, and Cellular, and Molecular Biology, University of Tennessee at Knoxville, Knoxville, Tennessee 37966, United States*

Sushil K. Satija − *Center for Neutron Research, National Institute of Standards and Technology, Gaithersburg, Maryland 20899, United States*

John F. Ankner − *Large-Scale Structures Group, Neutron Scattering Division, Oak Ridge National Laboratory, Oak Ridge, Tennessee 37830, United States;* orcid.org/0000-0002-6737-5718

Complete contact information is available at: https://pubs.acs.org/10.1021/acs.langmuir.9b03817

Author Contributions

[⊥]M.D.P., O.I.K., and N.G.B. contributed equally to this work.

Notes

The authors declare no competing financial interest.

ACKNOWLEDGMENTS

We thank Alessandro Mazza, Hugh O'Neill, and Shuo Qian (ORNL) for valuable discussion on the design of experiments; Ryan Beer and Bill Dougherty from Total Cray Valley for consulting, technical assistance, and SMA copolymer samples; and Candice Halbert for helping in setting up the Langmuir trough at BL4B. M.D.P acknowledges the funding support from Oak Ridge National Laboratory's (ORNL) Basic Energy Sciences−Scientific User Facilities (SNS & HFIR), Large Scale Structures Group−M&S and Travel, and in part by an appointment to the ORNL ASTRO program, sponsored by the U.S. Department of Energy and administered by the Oak Ridge Institute for Science and Education. This project was also funded by the Gibson Family Foundation, the UTK/ORNL Science Alliance, the Tennessee Plant Research Center, JDRD Award to B.D.B, the Dr. Donald L. Akers Faculty Enrichment Fellowship to B.D.B and National Science Foundation support to B.D.B (DGE-0801470 and EPS 1004083). Neutron experiments were conducted at Liquids Reflectometer (BL4B), Spallation Neutron Source, a DOE Office of Science User Facility operated by the ORNL.

REFERENCES

(1) Quinn, P.; Williams, W. The structural role of lipids in photosynthetic membranes. *Biochim. Biophys. Acta, Rev. Biomembr.* **1983**, *737*, 223−266.

(2) Andersson, B.; Anderson, J. M. Lateral heterogeneity in the distribution of chlorophyll-protein complexes of the thylakoid membranes of spinach chloroplasts. *Biochim. Biophys. Acta, Bioenerg.* **1980**, *593*, 427−440.

(3) MacGregor-Chatwin, C.; Sener, M.; Barnett, S. F.; Hitchcock, A.; Barnhart-Dailey, M. C.; Maghlaoui, K.; Barber, J.; Timlin, J. A.; Schulten, K.; Hunter, C. N. Lateral segregation of photosystem I in cyanobacterial thylakoids. *Plant Cell* **2017**, *29*, 1119−1136.

(4) Hasan, S. S.; Cramer, W. A. Internal lipid architecture of the hetero-oligomeric cytochrome b6f complex. *Structure* **2014**, *22*, 1008−1015.

(5) Jordan, P.; Fromme, P.; Witt, H. T.; Klukas, O.; Saenger, W.; Krauß, N. Three-dimensional structure of cyanobacterial photosystem I at 2.5 Å resolution. *Nature* **2001**, *411*, 909.

(6) Oluwole, A. O.; Danielczak, B.; Meister, A.; Babalola, J. O.; Vargas, C.; Keller, S. Solubilization of membrane proteins into functional lipid-bilayer nanodiscs using a diisobutylene/maleic acid copolymer. *Angew. Chem., Int. Ed.* **2017**, *56*, 1919−1924.

(7) Long, A. R.; O'Brien, C. C.; Malhotra, K.; Schwall, C. T.; Albert, A. D.; Watts, A.; Alder, N. N. A detergent-free strategy for the reconstitution of active enzyme complexes from native biological membranes into nanoscale discs. *BMC Biotechnol.* **2013**, *13*, 41.

(8) Denisov, I. G.; Sligar, S. G. Nanodiscs for structural and functional studies of membrane proteins. *Nat. Struct. Mol. Biol.* **2016**, *23*, 481.

(9) Pollock, N. L.; Lee, S. C.; Patel, J. H.; Gulamhussein, A. A.; Rothnie, A. J. Structure and function of membrane proteins encapsulated in a polymer-bound lipid bilayer. *Biochim. Biophys. Acta, Biomembr.* **2018**, *1860*, 809−817.

(10) Seddon, A. M.; Curnow, P.; Booth, P. J. Membrane proteins, lipids and detergents: not just a soap opera. *Biochim. Biophys. Acta, Biomembr.* **2004**, *1666*, 105−117.

(11) Popot, J.-L. Amphipols, nanodiscs, and fluorinated surfactants: three nonconventional approaches to studying membrane proteins in aqueous solutions. *Annu. Rev. Biochem.* **2010**, *79*, 737−775.

(12) Stubbs, G. W.; Litman, B. J. Effect of alterations in the amphipathic microenvironment on the conformational stability of bovine opsin. 1. Mechanism of solubilization of disk membranes by the nonionic detergent, octyl glucoside. *Biochemistry* **1978**, *17*, 215−219.

(13) Landreh, M.; Marty, M. T.; Gault, J.; Robinson, C. V. A sliding selectivity scale for lipid binding to membrane proteins. *Curr. Opin. Struct. Biol.* **2016**, *39*, 54−60.

(14) Prabudiansyah, I.; Kusters, I.; Caforio, A.; Driessen, A. J. Characterization of the annular lipid shell of the Sec translocon. *Biochim. Biophys. Acta, Biomembr.* **2015**, *1848*, 2050−2056.

(15) Dörr, J. M.; van Coevorden-Hameete, M. H.; Hoogenraad, C. C.; Killian, J. A. Solubilization of human cells by the styrene−maleic acid copolymer: Insights from fluorescence microscopy. *Biochim. Biophys. Acta, Biomembr.* **2017**, *1859*, 2155−2160.

(16) Orekhov, P. S.; Bozdaganyan, M. E.; Voskoboynikova, N.; Mulkidjanian, A. Y.; Steinhoff, H.-J.; Shaitan, K. V. Styrene/Maleic Acid Copolymers Form SMALPs by Pulling Lipid Patches out of the Lipid Bilayer. *Langmuir* **2019**, *35*, 3748−3758.

(17) Korotych, O.; Mondal, J.; Gattás-Asfura, K. M.; Hendricks, J.; Bruce, B. D. Evaluation of commercially available styrene-co-maleic acid polymers for the extraction of membrane proteins from spinach chloroplast thylakoids. *Eur. Polym. J.* **2019**, *114*, 485−500.

(18) Brady, N. G.; Li, M.; Ma, Y.; Gumbart, J. C.; Bruce, B. D. Non-detergent isolation of a cyanobacterial photosystem I using styrene maleic acid alternating copolymers. *RSC Adv.* **2019**, *9*, 31781−31796.

(19) Brady, N. G.; Qian, S.; Bruce, B. D. Analysis of styrene maleic acid alternating copolymer supramolecular assemblies in solution by small angle X-ray scattering. *Eur. Polym. J.* **2019**, *111*, 178−184.

(20) Breyton, C.; Tribet, C.; Olive, J.; Dubacq, J.-P.; Popot, J.-L. Dimer to Monomer Conversion of the Cytochrome b6f Complex: Causes and Consequences. *J. Biol. Chem.* **1997**, *272*, 21892−21900.
(21) Phan, M. D.; Kim, H.; Lee, S.; Yu, C.-J.; Moon, B.; Shin, K. HIV peptide-mediated binding behaviors of nanoparticles on a lipid membrane. *Langmuir* **2017**, *33*, 2590−2595.
(22) Phan, M. D.; Shin, K. Effects of Cardiolipin on Membrane Morphology: A Langmuir Monolayer Study. *Biophys. J.* **2015**, *108*, 1977−1986.
(23) Pardo, J. J. D.; Dörr, J. M.; Iyer, A.; Cox, R. C.; Scheidelaar, S.; Koorengevel, M. C.; Subramaniam, V.; Killian, J. A. Solubilization of lipids and lipid phases by the styrene−maleic acid copolymer. *Eur. Biophys. J.* **2017**, *46*, 91−101.
(24) Smaby, J. M.; Kulkarni, V. S.; Momsen, M.; Brown, R. E. The interfacial elastic packing interactions of galactosylceramides, sphingomyelins, and phosphatidylcholines. *Biophys. J.* **1996**, *70*, 868−877.
(25) Seeck, O.; Kaendler, I.; Tolan, M.; Shin, K.; Rafailovich, M.; Sokolov, J.; Kolb, R. Analysis of x-ray reflectivity data from low-contrast polymer bilayer systems using a Fourier method. *Appl. Phys. Lett.* **2000**, *76*, 2713−2715.
(26) Ankner, J. F.; Majkrzak, C. F. Subsurface profile refinement for neutron specular reflectivity. *Proc. SPIE* **1992**, 260−269.
(27) Doucet, M.; Leal, R. F.; Hobson, T. C. Web interface for reflectivity fitting. *SoftwareX* **2018**, *7*, 287−293.
(28) Parratt, L. G. Surface studies of solids by total reflection of X-rays. *Phys. Rev.* **1954**, *95*, 359.
(29) Tolan, M. *X-ray scattering from soft-matter thin films*; Springer, 1999.
(30) Vaknin, D.; Kjaer, K.; Als-Nielsen, J.; Lösche, M. Structural properties of phosphatidylcholine in a monolayer at the air/water interface: Neutron reflection study and reexamination of x-ray reflection measurements. *Biophys. J.* **1991**, *59*, 1325−1332.
(31) Williams, A. D.; Wilkin, J. M.; Dluhy, R. A. An investigation of miscibility in monolayer films of phosphocholine-phosphoglycerol binary mixtures. *Colloids Surf., A* **1995**, *102*, 231−245.
(32) Koppenol, S.; Yu, H.; Zografi, G. Mixing of saturated and unsaturated phosphatidylcholines and phosphatidylglycerols in monolayers at the air/water interface. *J. Colloid Interface Sci.* **1997**, *189*, 158−166.
(33) Bottier, C.; Géan, J.; Artzner, F.; Desbat, B.; Pezolet, M.; Renault, A.; Marion, D.; Vié, V. Galactosyl headgroup interactions control the molecular packing of wheat lipids in Langmuir films and in hydrated liquid-crystalline mesophases. *Biochim. Biophys. Acta, Biomembr.* **2007**, *1768*, 1526−1540.
(34) Hoyo, J.; Guaus, E.; Torrent-Burgués, J. Monogalactosyldiacylglycerol and digalactosyldiacylglycerol role, physical states, applications and biomimetic monolayer films. *Eur. Phys. J. E: Soft Matter Biol. Phys.* **2016**, *39*, 39.
(35) Gzyl-Malcher, B.; Filek, M.; Makyła, K. Langmuir monolayers of chloroplast membrane lipids. *Thin Solid Films* **2008**, *516*, 8844−8847.
(36) Watkins, E. B.; Frey, S. L.; Chi, E. Y.; Cao, K. D.; Pacuszka, T.; Majewski, J.; Lee, K. Y. C. Enhanced Ordering in Monolayers Containing Glycosphingolipids: Impact of Carbohydrate Structure. *Biophys. J.* **2018**, *114*, 1103−1115.
(37) Swainsbury, D. J.; Scheidelaar, S.; Foster, N.; Van Grondelle, R.; Killian, J. A.; Jones, M. R. The effectiveness of styrene-maleic acid (SMA) copolymers for solubilisation of integral membrane proteins from SMA-accessible and SMA-resistant membranes. *Biochim. Biophys. Acta, Biomembr.* **2017**, *1859*, 2133−2143.
(38) Orwick, M. C.; Judge, P. J.; Procek, J.; Lindholm, L.; Graziadei, A.; Engel, A.; Gröbner, G.; Watts, A. Detergent-Free Formation and Physicochemical Characterization of Nanosized Lipid−Polymer Complexes: Lipodisq. *Angew. Chem., Int. Ed.* **2012**, *51*, 4653−4657.

https://dx.doi.org/10.1021/acs.langmuir.9b03817
Langmuir 2020, 36, 3970−3980